Preprints of the 21st IFAC World Congress (Virtual)
Berlin, Germany, July 12-17, 2020

On the global feedback stabilization of regenerative optical amplifiers

A. Deutschmann * **W. Kemmetmüller** * **A. Kugi** *,**

* *Automation and Control Institute, Complex Dynamical Systems Group, TU Wien, Vienna, Austria*
** *Center for Vision, Automation & Control, Austrian Institute of Technology, Vienna, Austria*

Abstract: The generation of high-energy laser pulses by so-called regenerative (optical) amplifiers is limited by the occurrence of period-doubling bifurcations induced by an inherently unstable pulse-to-pulse dynamics. Recently, the application of linear feedback methods to stabilize this pulse-to-pulse dynamics by modifying the supplied seed pulses was suggested as an alternative to the quite expensive current state of the art involving dedicated pre-amplifiers. To address some shortcomings inherent to the linear feedback, this paper investigates the design of nonlinear state feedback laws and in particular the possibility to stabilize the pulse-to-pulse dynamics globally subject to the given input constraints.

Keywords: Regenerative amplifiers, pulsed laser systems, global asymptotic stability, constrained nonlinear control

1. INTRODUCTION

Ultra-short pulses of intense laser light have become an essential tool in many scientific areas such as strong field physics (see Krausz and Ivanov (2009)), coherent light-matter interactions as investigated in Goswami (2003), for pumping of optical parametric amplifiers and free electron lasers (see, e.g., Malevich et al. (2013) and Kellert et al. (2013)). Chapman et al. (2011) proposed the use of such pulses for the crystallographic analysis of fragile protein structures. Due to the high power density, short high-energy pulses are used for ablation-based material processing of micro-mechanical devices (e.g., in Nolte et al. (1997); Tönshoff et al. (2000); Jiang et al. (2018)) and laser-based eye surgery (e.g., in Sekundo et al. (2008)).

The generation of high-energy pulses is usually done by feeding seed pulses with low pulse energy into so-called regenerative amplifiers (RAs), where a continuously pumped gain medium is placed inside an optical resonator. The pulse is then cycled several times until the stored energy of the gain medium is extracted and the amplified pulse is released. Since the pumping process is typically not strong enough to fully recharge the gain medium between two consecutive pulses, the amplification characteristics of the current pulse depends on the previous pulse and a pulse-to-pulse dynamic emerges. The seed pulses are injected into the resonator with a fixed periodicity and thus the amplifier approaches a steady state where the pumping process exactly compensates the energy extracted by the previous pulse. When trying to exploit the full potential of a given amplifier, it has to be operated close to the damage threshold of the cavity optics. An uncontrolled excitation of the pulse-to-pulse dynamics is thus potentially hazardous. The coupling of consecutive pulses described above can even render the amplifier unstable in certain operational regions as analyzed by Dörring et al. (2004); Grishin et al. (2007). Unfortunately, these regions usually contain interesting operating points such as the point of highest energy extraction and the point of highest energy efficiency. A simple but rather costly solution to this problem proposed by Grishin et al. (2009) is to increase the available seed energy using dedicated pre-amplifiers. While this has become the standard approach today, an early work by Dörring et al. (2004) already indicated the possibility of feedback methods to stabilize such operational regimes. Recently, Deutschmann et al. (2019) presented a first implementation of feedback approaches by modifying the energy of the seed pulses using programmable optical filters. Such filters are commonly employed in different applications, e.g., to compensate for gain-narrowing and pulse propagation effects in Malevich et al. (2013), or to iteratively generate output pulses of arbitrary shape in Deutschmann et al. (2018).

The experimental and numerical analysis of the linear output feedback laws in Deutschmann et al. (2019) illustrates their sensitivity with respect to disturbances due to the nonlinearity of the output map. Since it is possible to infer the system's state directly from measurements of the residual pumping beam, application of state feedback methods can increase the robustness of the closed-loop system. However, for operating points in a highly nonlinear regime, the region of attraction of linear feedback designs becomes quite small. Therefore, it seems natural to investigate the design of a nonlinear controller which ensures global asymptotic stability (GAS) of the closed-loop system. This paper exactly pursues this goal.

To this end, the mathematical model is briefly summarized in Section 2 and a motivating example is given in Section 3. Section 4 investigates the design of nonlinear feedback laws and their limitations in practice. Finally, a short conclusion is given in Section 5.

2. MATHEMATICAL MODEL

This section shortly summarizes the mathematical model of the regenerative amplifier. For more details, the reader is referred to Deutschmann et al. (2019); Deutschmann (2019). Since we are mainly interested in the pulse-to-pulse dynamics, the laser pulses can be described using the intensity $I(t)$ while neglecting their spectral properties. Without loss of generality, we consider regenerative amplifiers using a simple atomic four-level structure of the gain medium and a ring cavity design as illustrated in Fig. 1, i.e., the laser pulse passes the gain medium once per round trip. Additionally, the amplifier is operated in a so-called end-pumped configuration, i.e., the gain medium is excited using a continuous pumping beam $I_\mathrm{P}(t)$ which is fed through the gain medium axially aligned with the laser pulses and propagates in the same direction.

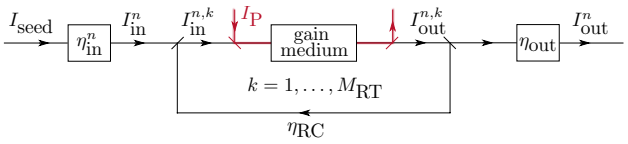

Fig. 1. Schematic overview of a regenerative amplifier.

As a result, identical seed pulses $I_\mathrm{seed}(t)$ from a source with repetition rate f_rep are fed through an optical filter with an adjustable input loss factor $0 \leq \eta_\mathrm{in}^n \leq 1$ which can be modified for each pulse with index n. The resulting input pulse is thus given by

$$I_\mathrm{in}^n(t) = \eta_\mathrm{in}^n I_\mathrm{seed}(t). \tag{1}$$

Denoting the k-th round trip inside the cavity of the n-th pulse by $I_\mathrm{in}^{n,k}(t)$ and $I_\mathrm{out}^{n,k}(t)$ according to Fig. 1, the modified input pulse $I_\mathrm{in}^n(t)$ is then injected into the cavity, i.e., $I_\mathrm{in}^{n,1}(t) = I_\mathrm{in}^n(t)$. Aligning the propagation direction with the z-axis and using the population inversion of the excited states ΔN, each amplification process in the gain medium can be described using the coupled set of (partial) differential equations, see Deutschmann et al. (2019),

$$\frac{\partial I}{\partial t} = -v\frac{\partial I}{\partial z} + \sigma v \Delta N\, I \tag{2a}$$

$$\frac{\partial I_\mathrm{P}}{\partial t} = -v_\mathrm{P}\frac{\partial I_\mathrm{P}}{\partial z} - \sigma_\mathrm{P} v_\mathrm{P}\left(N_\mathrm{dop} - \Delta N\right) I_\mathrm{P} \tag{2b}$$

$$\frac{\partial \Delta N}{\partial t} = -\gamma \Delta N - \frac{\sigma I}{\hbar\omega}\Delta N + \frac{\sigma_\mathrm{P} I_\mathrm{P}}{\hbar\omega_\mathrm{P}}\left(N_\mathrm{dop} - \Delta N\right), \tag{2c}$$

with the reduced Planck constant $\hbar$, the relaxation rate γ, the density of the dopant N_dop and the associated group velocities v, v_P, the atomic transition cross-sections σ, σ_P, and the corresponding angular frequencies ω, ω_P, respectively. For each round trip k, the input pulse enters the gain medium on the left boundary $I(0,t) = I_\mathrm{in}^{n,k}(t)$ with the initial condition $I(z,0) = 0$. The amplified output pulse is given by $I_\mathrm{out}^{n,k} = I(L,t)$ with the length of the gain medium L. Similarly, it follows for the continuous pumping beam that $I_\mathrm{P}(0,t) = {}^{p_\mathrm{pump}(t)}/_{A_B}$ with the (slowly) adjustable pump power $p_\mathrm{pump}(t)$ and the beam cross sectional area A_B. Since the pump power is changing slowly, it is assumed that its initial value $I_\mathrm{P}(z,0)$ is a steady-state solution of (2b). Finally, the population inversion couples the successive round trips in the form $\Delta N(z,0) = \Delta N_{rem}^{n,k-1}(z)$, with the remaining population inversion of the previous round trip $\Delta N_{rem}^{n,k-1}(z)$. After M_RT round trips, the amplified output pulse is finally given by

$$I_\mathrm{out}^n(t) = \eta_\mathrm{out} I_\mathrm{out}^{n,M_\mathrm{RT}}(t) \tag{3}$$

with the output loss factor η_out. For the remaining time until the next pulse $I_\mathrm{in}^{n+1}(t)$ arrives, the cavity remains empty (i.e., $I(z,t) = 0$) and the population inversion is able to regenerate according to (2) to obtain the initial population inversion of the next pulse $\Delta N_\mathrm{in}^n(z) = \Delta N_\mathrm{rem}^{n+1,0}(z)$.

In case this regeneration process is not able to fully restore the initial population inversion, the current behavior of the regenerative amplifier depends on the previous pulses which results in a coupling of consecutive pulses. By using time-scale separation and singular perturbation approaches as shown in Deutschmann et al. (2019), this pulse-to-pulse dynamics of (2) can be described by a nonlinear discrete-time dynamic system

$$x^{n+1} = f(x^n, u^n; p^n) \tag{4a}$$

$$y^n = h(x^n, u^n), \tag{4b}$$

with the dynamic map f and the output map h using

$$x^n = \exp\left(\sigma \int_0^L \Delta N_\mathrm{in}^n(z)\mathrm{d}z\right), \tag{5a}$$

$$u^n = A_\mathrm{B}\int_0^\infty I_\mathrm{in}^n(\xi)\mathrm{d}\xi, \quad y^n = A_\mathrm{B}\int_0^\infty I_\mathrm{out}^n(\xi)\mathrm{d}\xi. \tag{5b}$$

Additionally, it has been be assumed that the pump power remains approximately constant for the time between two consecutive pulses, i.e., $p_\mathrm{pump}(t) \approx p^n$ for $t \in [t^n, t^{n+1})$ with $t^{n+1} = t^n + {}^1/_{f_\mathrm{rep}}$. Note that f and h are quite complex iterative relations which can be found in Deutschmann et al. (2019); Deutschmann (2019). From a physical perspective, the state variable x according to (5a) denotes the so-called initial "small signal" gain of the gain medium during a single pass of the laser pulse while u and y denote the total energy of the input and output pulses, respectively.

The corresponding initial condition x^0 of the discrete-time system (4) is defined by the initial population inversion $\Delta N_\mathrm{in}^0(z)$ according to (5a). By integration of (1) and multiplying the result with cross sectional area A_B, the input u^n can be expressed as a function of the adjustable input loss factor of the optical filter as $u^n = \eta_\mathrm{in}^n W_\mathrm{seed}$ with the available energy of the seed pulses W_seed. Since $0 \leq \eta_\mathrm{in}^n \leq 1$, it follows that the system is subject to the input constraint

$$0 \leq u^n \leq \bar{u}, \tag{6}$$

with $\bar{u} = W_\mathrm{seed}$.

Regenerative amplifiers are used to generate a train of identical high-energy pulses most of the time. The dynamic model (4) is thus operated at a steady state x^s given by

$$x^s = f(x^s, u^s; p^s), \tag{7}$$

with the corresponding steady-state values u^s, p^s and

$$y^s = h(x^s, u^s). \tag{8}$$

Due to the scalar nature of the state, the dynamic and output map according to (4) and the solution of (7) can be illustrated as shown in Fig. 2 for different pump powers p. When the steady state x^s moves into the steep declining section of f, the amplifier becomes unstable and the output trajectory converges to periodic orbits (except for chaotic points as analyzed in Grishin et al. (2007) using a simpler

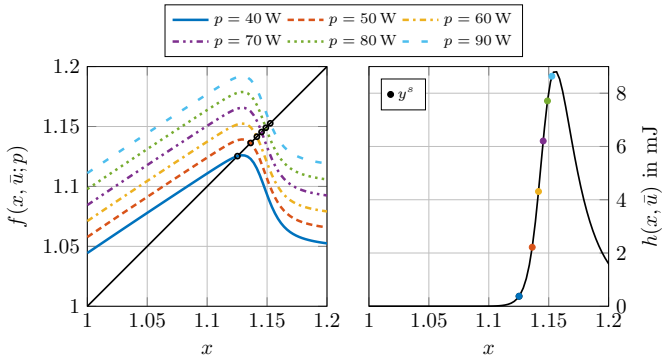

Fig. 2. Dynamic map f and output map h for $u^s = \bar{u}$ and different pump powers p: the solutions x^s of (7) and the corresponding outputs y^s are marked by dots.

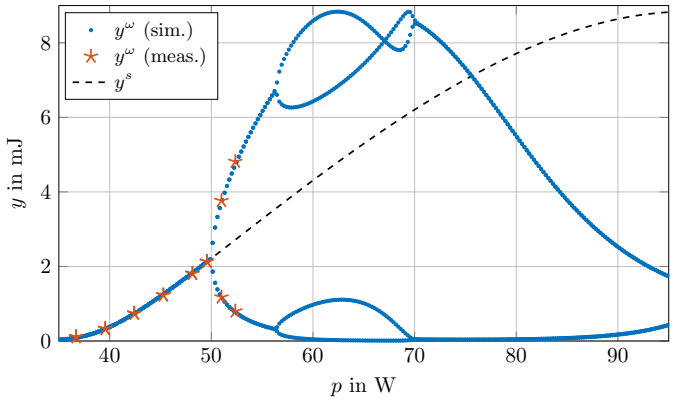

Fig. 3. Simulated ω-limit set of the output y^ω due to the unstable dynamics of the regenerative amplifier at higher pump powers p compared to the steady-state output y^s (dashed line) and measurements from a Yb:CaF2-based experimental amplifier.

model). The resulting limit set exhibits so-called period-doubling bifurcations shown in Fig. 3. This figure also shows that the model (4) is in excellent agreement with measurement data from a Yb:CaF2-based experimental amplifier.

Remark 1. To obtain this high level of agreement between simulation and measurement data as shown in Fig. 3, detailed properties of the physical setup (e.g., the quasi-three-level nature of Yb:CaF2, a multi-pass pumping scheme, etc.) have to be considered. Due to space limitation, these details are omitted in this work. The presented results, however, can be transferred directly to this more complicated case. The interested reader is referred to Deutschmann (2019) for more details on this topic.

3. A MOTIVATING EXAMPLE

The amplifier according to Fig. 3 is designed for pulse energies up to approximately 6 mJ and any open-loop operation above 55 W pump power may damage its intracavity optics. Additionally, a stable operation is limited to approximately 2 mJ output pulses while a steady-state operation up to 70 W pump power would be possible by either increasing the seed energy, which is the current state of art but requires an additional pre-amplifier, or by stabilizing the amplifier using feedback. The latter was recently proposed by Deutschmann et al. (2019) including

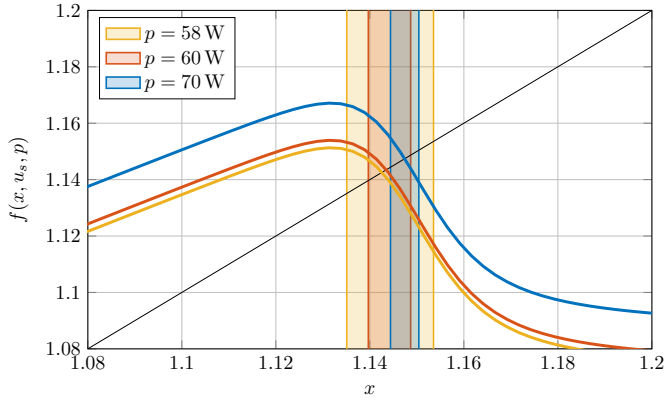

Fig. 4. Numerical analysis of the region of attraction. The shaded areas indicate the largest set of initial values x^0 around the desired steady state from which the closed loop converges to the steady state x^s using the linear output feedback law (9).

experimental results using a dynamic output feedback law of the form

$$u^{n+1} = u^s + \varsigma\left(\boldsymbol{k}_{\mathrm{FB}}^T \begin{bmatrix} y^n - y^s \\ u^n - u^s \end{bmatrix}\right), \tag{9}$$

with the strictly monotonous sigmoid function $\varsigma : \mathbb{R} \mapsto [-u^s, \bar{u} - u^s]$ to satisfy the input constraints (6). A suitable linear feedback gain $\boldsymbol{k}_{\mathrm{FB}}$ can be obtained by transforming (4) into sensor coordinates, i.e., by substituting x^n by y^n in the vicinity of any x^n where h can be inverted locally.

Simulation scenarios using the detailed model (2) together with the feedback law (9) show a satisfying behavior of the closed-loop system up to roughly 55 W pump power, which is confirmed by the experimental implementation in Deutschmann et al. (2019). For higher pump powers p, where the amplifier becomes increasingly unstable and nonlinear, the region of attraction of such linear feedback designs decreases rapidly as illustrated in Fig. 4. Moreover, the convergence behavior starts to become significantly non-monotonic as one approaches the region of attraction's borders, which can produce transient pulse energies far off the steady-state as shown in Fig. 5. As a result, the behavior of the closed-loop system is quite sensitive to disturbances such as fluctuations of the emitted power of the pumping laser or of the energy of the seed pulses.

To operate amplifiers safely at pumping levels where a failure of the feedback stabilization is potentially damaging to the cavity optics, one requires feedback laws that exhibit a certain level of robustness and ideally guarantee stability of the closed-loop system. Since the state x can be estimated directly by using measurements of the transmitted pumping beam, it seems quite natural to apply state feedback methods and design nonlinear feedback laws based on the model (4) that systematically account for the input constraints (6).

4. NONLINEAR STATE FEEDBACK

We are looking for a state feedback $u^k = g(x^k) : \mathcal{X} \mapsto [0, \bar{u}]$ such that the closed-loop system $x^{k+1} = f_{\mathrm{CL}}(x^k) = f(x^k, g(x^k))$ exhibits a desired behavior and is globally asymptotically stable (GAS). Notice that the dependence on p is omitted for clarity. Without loss of generality, we

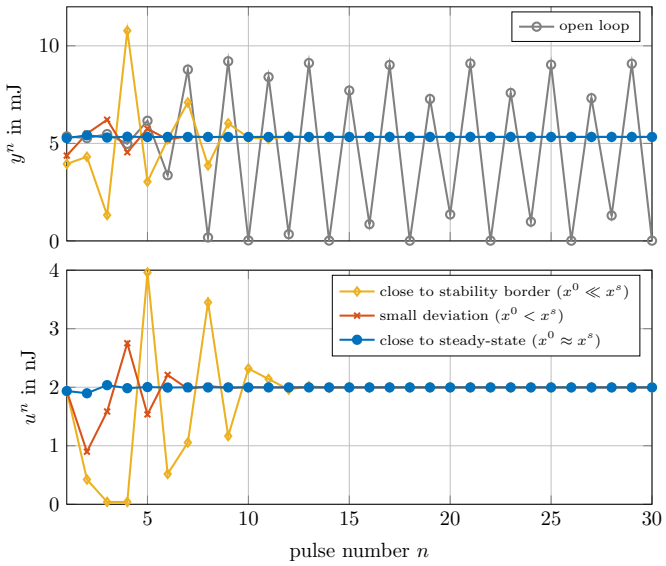

Fig. 5. Dynamic behavior of the controlled and uncontrolled regenerative amplifier for $p = 65\,\mathrm{W}$.

restrict the following considerations to scenarios where energy is stored inside the gain medium initially, i.e., $x^0 \geq 1$, and the pumping beam is active, i.e., $p > 0$. By the definition of $f(x,u)$ it is clear that $f(x,u) > 1$ for $x > 1$. This is quite intuitive, since the incoming laser pulses can only extract energy as long as the laser medium has some population inversion left. As a result, the dynamics of the system is restricted to the domain $x \in \mathcal{X} = [1, \infty)$.

Since we are interested in continuous feedback functions g, the discrete-time nature of the dynamics (4) implies that the closed-loop system is GAS if $f_{\mathrm{CL}}(x)$ is a contraction map, i.e.,

$$|f_{\mathrm{CL}}(x_1) - f_{\mathrm{CL}}(x_2)| \leq c\,|x_1 - x_2| \tag{10}$$

holds for all $x_1, x_2 \in [1, \infty)$ with $c < 1$. This can be easily seen by using the Lyapunov function $V(e^k) = |e^k|$ with $e^k = x^k - x^s$ where $x^s = f_{\mathrm{CL}}(x^s)$. Applying Lyapunov's direct method for discrete-time systems (see, e.g., Freeman (1965)) directly results in

$$\begin{aligned} V(e^{k+1}) - V(e^k) &= |f_{\mathrm{CL}}(x^k) - x^s| - |x^k - x^s| \\ &< (c-1)|x^k - x^s| < 0. \end{aligned} \tag{11}$$

Since $f_{\mathrm{CL}}(x)$ is differentiable, the condition (10) is satisfied iff

$$\left| \frac{\mathrm{d}f_{\mathrm{CL}}}{\mathrm{d}x}(x) \right| \leq c < 1 \tag{12}$$

for all x. Differentiating the closed-loop dynamics with respect to x yields

$$\frac{\mathrm{d}f_{\mathrm{CL}}}{\mathrm{d}x}(x) = \frac{\partial f}{\partial x}(x, g(x)) + \frac{\partial f}{\partial u}(x, g(x)) \frac{\mathrm{d}g}{\mathrm{d}x}(x), \tag{13}$$

which is why a desired $f_{\mathrm{CL}}^{\mathrm{d}}(x)$ can be obtained by solving the differential equation

$$\frac{\mathrm{d}g}{\mathrm{d}x} = \left(\frac{\partial f}{\partial u}(x,g) \right)^{-1} \left(\frac{\mathrm{d}f_{\mathrm{CL}}^{\mathrm{d}}}{\mathrm{d}x}(x,g) - \frac{\partial f}{\partial x}(x,g) \right) \tag{14}$$

with respect to g in the vicinity of any point $(x,g) \in \mathcal{X} \times [0, \bar{u}]$ with $\frac{\partial f}{\partial u}(x,g) \neq 0$. This formulation is particular beneficial since it is much simpler to give desired values for $\frac{\mathrm{d}f_{\mathrm{CL}}^{\mathrm{d}}}{\mathrm{d}x}(x,g)$ than for $f_{\mathrm{CL}}^{\mathrm{d}}(x)$ itself.

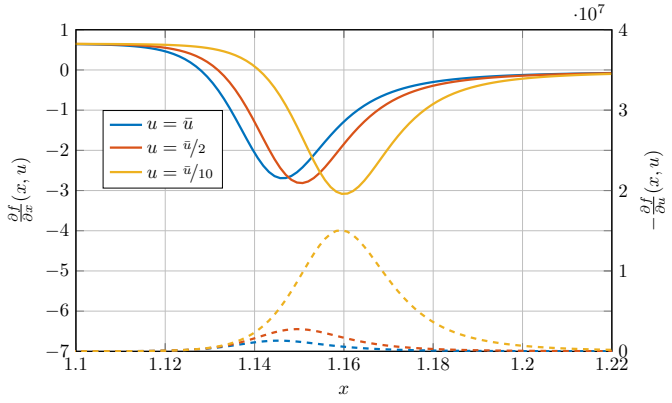

Fig. 6. Exemplary behavior of $\frac{\partial f}{\partial x}(x,u)$ (solid) and $\frac{\partial f}{\partial u}(x,u)$ (dashed) for input pulses $u \in \{\bar{u}/10, \bar{u}/2, \bar{u}\}$.

4.1 Global asymptotic stabilization

Since $\frac{\partial f}{\partial u}(x,g) < 0$ for all values inside the region of interest except for points on the domain boundaries $x = 1$ and $x \to \infty$, we can solve (14) starting from the initial condition

$$g(1) = \bar{u} \tag{15}$$

while ensuring that the desired correction $\frac{\mathrm{d}f_{\mathrm{CL}}^{\mathrm{d}}}{\mathrm{d}x}(x,g) - \frac{\partial f}{\partial x}(x,g)$ becomes sufficiently small when approaching the domain boundaries. This is easily possible since the amplifier's natural behavior $\frac{\partial f}{\partial x}(x,g)$ only starts to violate the stability condition (12) far off the boundaries. An exemplary behavior of $\frac{\partial f}{\partial x}(x,u)$ and $\frac{\partial f}{\partial u}(x,u)$ is depicted in Fig. 6. Since the regions where the amplifier becomes unstable are aligned with those regions where $\frac{\partial f}{\partial u}(x,u)$ is large, shaping the closed-loop system in an arbitrary way is quite difficult and requires large control efforts. In contrast, stabilizing a certain operating point locally is rather easy. While it is expected (cf. Grishin et al. (2009)) that lower energies of the input pulse tend to destabilize the amplifiers, it is interesting to note that this also corresponds to an increased influence of the input on the amplifier's dynamics.

To stabilize the amplifier globally, one can choose

$$\frac{\mathrm{d}f_{\mathrm{CL}}^{\mathrm{d}}}{\mathrm{d}x}(x,g) = \begin{cases} 1 - \varepsilon & \text{for } \frac{\partial f}{\partial x}(x,g) \leq 1 - \varepsilon \\ \frac{\partial f}{\partial x}(x,g) & \text{else} \end{cases} \tag{16}$$

with a small stability margin $\varepsilon > 0$. A resulting solution $g(x)$ of (14) with (15) and (16) and the corresponding closed loop dynamics $f_{\mathrm{CL}}(x)$ is illustrated in Fig. 7.

Remark 2. Obtaining a numerical solution of (14) can be quite difficult when approaching the lower limit $u = 0$ and thus the usage of implicit schemes is beneficial.

Although decreasing the input is increasing its influence on the amplifier's dynamics (cf. Fig. 6), one is typically not able to arbitrarily shape the closed-loop dynamics since the one-sided limit $\lim_{u \to 0^+} \frac{\partial f}{\partial u}(x,u)$ is bounded and thus the corrective action of the feedback law adhering to the input constraints remains limited (see (14)). The complexity and semi-analytic formulation of the dynamic map $f(x,u)$ makes it quite difficult to give strict results on the integrability of (14) over $\mathcal{X}$ subject to (6) for arbitrary amplifiers. Nevertheless, simulation results suggest that

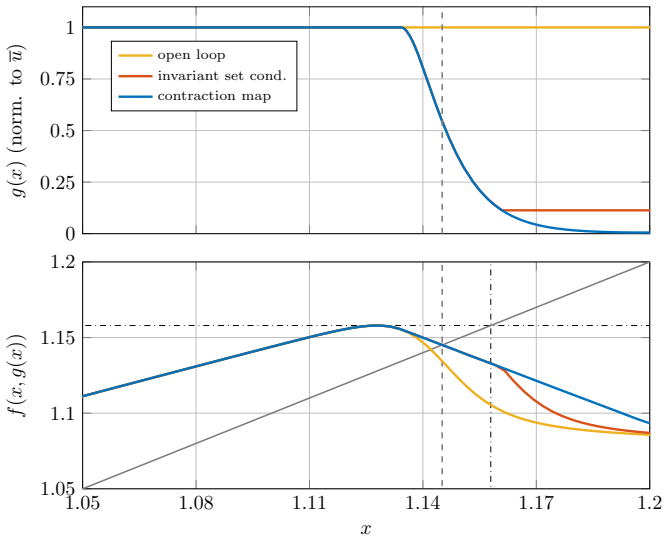

Fig. 7. Globally stabilizing feedback $u^k = g(x^k)$ according to (14), (15), and (16) and the resulting closed-loop dynamics $f_{\mathrm{CL}}(x) = f(x, g(x))$ for $p = 65\,\mathrm{W}$ and $\varepsilon = 0.03$. The contraction map case strictly fulfills (12) while the invariant set case uses the relaxed condition (17).

one can indeed always choose an $\varepsilon > 0$ such that a GAS feedback law $g(x)$ exists.

Since $f_{\mathrm{CL}}(x)$ is bounded from above, as shown in Fig. 7, it is clear that $\mathcal{I} = \left[1, \bar{f}_{\mathrm{CL}}\right]$ with $\bar{f}_{\mathrm{CL}} = \max_{x \in \mathcal{X}} f_{\mathrm{CL}}(x)$ is an invariant set of the closed-loop dynamics, i.e., $f_{\mathrm{CL}}(\mathcal{I}) \subset \mathcal{I}$. If one ensures that $\frac{\mathrm{d}f_{\mathrm{CL}}}{\mathrm{d}x} < 0$ for all $x \notin \mathcal{I}$, i.e., $x > \bar{f}_{\mathrm{CL}}$, which is naturally fulfilled by keeping $g(x)$ constant when using a feedback design as given above, the closed-loop dynamics maps all states greater than $\bar{f}_{\mathrm{CL}}$ into the invariant set $\mathcal{I}$, i.e., $f_{\mathrm{CL}}(\mathcal{X} \setminus \mathcal{I}) \in \mathcal{I}$. From a stabilization perspective, it is thus sufficient to replace (12) by

$$\left|\frac{\mathrm{d}f_{\mathrm{CL}}}{\mathrm{d}x}(x)\right| < 1 \text{ for } x \in \mathcal{I} \text{ and } \frac{\mathrm{d}f_{\mathrm{CL}}}{\mathrm{d}x} < 0 \text{ else} \tag{17}$$

as illustrated in Fig. 7.

The main benefit of this invariant set condition becomes obvious when one considers the physical realization of such feedback strategies. First of all, the characteristics of optical filters is quite nonlinear and sensitive to errors at very low transmission factors $\eta_{\mathrm{in}} \ll 1$. Additionally, randomly scattered light pulses and background noise starts to become dominant compared to very small input pulses u^s at such operating points. The invariant set condition can thus be seen as a lower bound on the required actuation capabilities of the optical filters such that globally stabilizing feedback laws can be realized in practice.

This becomes particularly relevant if one considers the resulting feedback law for different levels of pump power p as shown in Fig. 8. While the shape of the feedback law itself remains unchanged, the required corrective action to ensure the contraction property of (17) at higher pump powers p increasingly shifts the steady-state input u^s and the required actuation capabilities towards very low values. For example, to globally stabilize the given amplifier at $p = 75\,\mathrm{W}$, one requires the input filter to

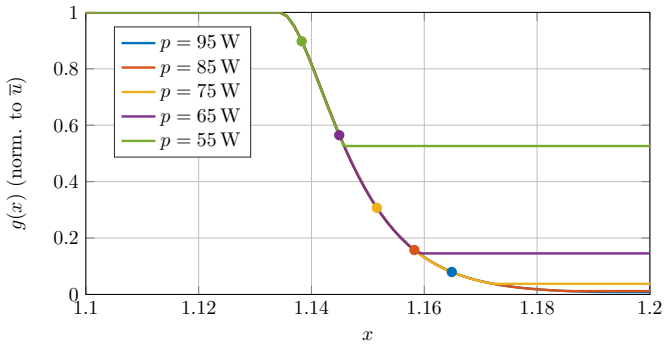

Fig. 8. Required feedback $g(x)$ with (16) and $\varepsilon = 0.03$ to satisfy (17) for different pump powers p. Dots indicate the resulting steady-state inputs u^s of the closed-loop system.

accurately produce input pulses down to approximately 4% of the seed pulse in total energy.

4.2 Highly saturated amplifiers

As we have seen above, trying to globally stabilize amplifiers by feedback methods may not be a practical solution for high pumping levels. However, highly saturated amplifiers have properties that can be beneficial for certain applications, e.g., as in Kroetz et al. (2015). Moreover, practical feedback laws are usually evaluated by more criteria than merely ensuring global asymptotic stability, such as the rejection of disturbances in the vicinity of the steady state.

In such cases, one can still use a nonlinear controller design based on (14) to stabilize a desired operating point (x^s, u^s) according to (7) by replacing the initial condition (15) with

$$g(x^s) = u^s \tag{18}$$

and solving (14) in both directions $x > x^s$ and $x < x^s$. If the upper input constraint of (6) is violated, $u^n = g(x^n)$ is set to the corresponding boundary value $\bar{u}$. Furthermore, one can modify (16) to adjust the decay of perturbations in the vicinity of x^s using

$$\frac{\mathrm{d}f_{\mathrm{CL}}^{\mathrm{d}}}{\mathrm{d}x}(x, g) = \begin{cases} 1 - \varepsilon & \text{for } \frac{\partial f}{\partial x}(x, g) \leq 1 - \varepsilon \\ \kappa & \text{for } f(x, g) - x \leq \delta \\ \frac{\partial f}{\partial x}(x, g) & \text{else,} \end{cases} \tag{19}$$

with the desired decay rate κ for all $|x - x^s| \leq \delta$. A solution of (14), (18), and (19) for $p = 85\,\mathrm{W}$ and a chosen $u^s = 4/10\ \bar{u}$ using $\varepsilon = 0.03$, $\delta = 0.05$, and $\kappa = -0.25$ is shown in Fig. 9. Clearly, by raising the steady-state input due to (18) compared to (15) (see Fig. 8), the resulting feedback law has not sufficient control margin with respect to the upper input constraint to stabilize the amplifier globally.

Operating points close to the maximum of $h(x, u)$ (roughly $x^s \approx 1.15$, cf. Fig. 2) are a natural choice if one is aiming for low fluctuations of the resulting output pulses. Since such operating points are usually located within or close to the unstable operating regime, one is bound to feedback schemes to stabilize the amplifier. One typical source of disturbances are fluctuations of the pump power p_{pump}. Simulation scenarios for fluctuations with a standard deviation of 1% of the nominal value are shown in Fig. 10. Since the globally stabilizing feedback law spends most

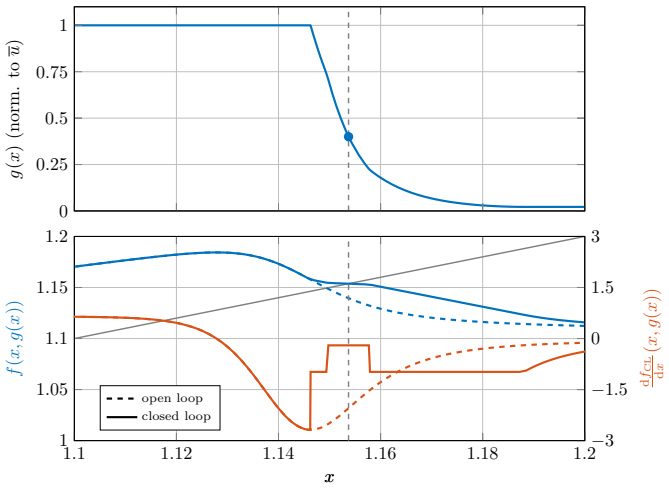

Fig. 9. A locally stabilizing solution of (14) with (18) and (19) for a pumping power of $p = 85\,\mathrm{W}$ and a chosen $u^s = {}^4\!/_{10}\ \bar{u}$ using $\varepsilon = 0.03$, $\delta = 0.05$ and $\kappa = -0.25$.

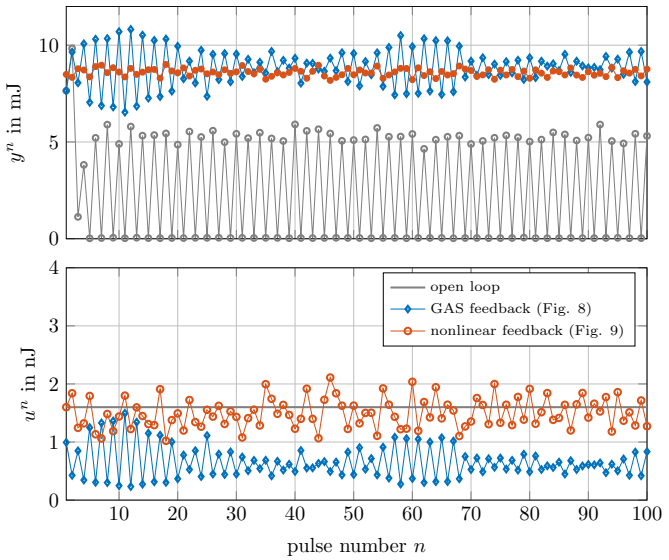

Fig. 10. Comparison of local and global feedback laws (cf. Fig. 8 and Fig. 9) for an amplifier operated at $p = 85\,\mathrm{W}$ close to the maximum of the output map h.

of the available control effort to ensure stability, the high level of pumping ($p = 85\,\mathrm{W}$) results in quite low values of u^n. Conversely, the feedback law given in Fig. 9 puts more effort into achieving a strongly damped behavior in the vicinty of the steady state x^s and thus rejects the disturbances of the pump power significantly better at the cost of local stability only.

Remark 3. An adjustable decay as in (19) can be combined with GAS feedback laws using the initial condition (15), but this further increases the corrective action of the feedback law and thus shifts the resulting u^s to even lower values. However, this is clearly a reasonable approach for low pump powers where u^s remains sufficiently far away from the lower input constraint.

5. CONCLUSIONS

This paper presents nonlinear state feedback laws for optical regenerative amplifiers to (globally) stabilize their pulse-to-pulse dynamics. By relating the derivative of the feedback law with the derivative of the desired closed-loop dynamics, one is able to design feedback laws that ensure global asymptotic stabilization (GAS) of the amplifier. Achieving GAS of the closed-loop system for a given amplifier indeed seems to be always possible. However, the limited capabilities of typical input filters restrict the applicability of such laws to low pump powers. Nevertheless, the same nonlinear design approach can be used to shape the closed-loop system locally while keeping a desired steady-state input.

REFERENCES

Chapman, H.N. et al. (2011). Femtosecond X-ray protein nanocrystallography. *Nature*, 470(7332), 73–77.

Deutschmann, A. (2019). *Modeling and Control of Optical Pulse Amplifiers for Ultra-Short Laser Pulses.* Phd thesis, TU Wien, Vienna, Austria.

Deutschmann, A. et al. (2018). Modeling and Iterative Pulse-Shape Control of Optical Chirped Pulse Amplifiers. *Automatica*, 98, 150–158.

Deutschmann, A. et al. (2019). Bifurcation suppression in regenerative amplifiers by active feedback methods. *submitted to Optics Express.*

Dörring, J. et al. (2004). Period doubling and deterministic chaos in continuously pumped regenerative amplifiers. *Optics Express*, 12(8), 1759–1768.

Freeman, H. (1965). *Discrete-Time Systems.* Wiley, Hoboken, USA.

Goswami, D. (2003). Optical pulse shaping approaches to coherent control. *Physics Reports*, 374(6), 385–481.

Grishin, M. et al. (2007). Dynamics of high repetition rate regenerative amplifiers. *Optics Express*, 15(15), 9434–9443.

Grishin, M. et al. (2009). Bifurcation suppression for stability improvement in Nd:YVO_4 regenerative amplifier. *Optics Express*, 17(18), 15700–15708.

Jiang, L. et al. (2018). Electrons dynamics control by shaping femtosecond laser pulses in micro/nanofabrication: Modeling, method, measurement and application. *Light: Science & Applications*, 7(2), 17134.

Kellert, M. et al. (2013). High power femtosecond 1030nm burst-mode front-end and pre-amplifier for the European XFEL pump-probe laser development. In *Proc. of the 2013 CLEO Europe/IQEC.* Munich.

Krausz, F. and Ivanov, M. (2009). Attosecond physics. *Reviews of Modern Physics*, 81(1), 163–234.

Kroetz, P. et al. (2015). Overcoming bifurcation instability in high-repetition-rate Ho:YLF regenerative amplifiers. *Optics Letters*, 40(23), 5427–5430.

Malevich, P. et al. (2013). High energy and average power femtosecond laser for driving mid-infrared optical parametric amplifiers. *Optics Letters*, 38(15), 2746–2749.

Nolte, S. et al. (1997). Ablation of metals by ultrashort laser pulses. *Journal of the Optical Society of America B*, 14(10), 2716–2722.

Sekundo, W. et al. (2008). First efficacy and safety study of femtosecond lenticule extraction for the correction of myopia: Six-month results. *Journal of Cataract & Refractive Surgery*, 34(9), 1513–1520.

Tönshoff, H.K. et al. (2000). Microdrilling of metals with ultrashort laser pulses. *Journal of Laser Applications*, 12(1), 23–27.